Nonlinear characterization of $Ge_{28}Sb_{12}Se_{60}$ bulk and waveguide devices

Molly R. Krogstad,[1,*] Sungmo Ahn,[2] Wounjhang Park,[2] and Juliet T. Gopinath[1,2]

[1]*Department of Physics, University of Colorado, Boulder, Colorado, 80309, USA*
[2]*Department of Electrical, Computer, and Energy Engineering, University of Colorado, Boulder, Colorado, 80309, USA*
[*]*molly.krogstad@colorado.edu*

Abstract: Single-mode $Ge_{28}Sb_{12}Se_{60}$ strip waveguides, fabricated with thermal evaporation and lift-off, were demonstrated at 1.03 μm. The linear and nonlinear optical properties of these waveguides were shown to be similar to bulk samples, with differences attributed to small variations in composition of ~4 atomic % or less. From z-scan measurements at 1.03 μm using circularly polarized, ~200 fs pulses at 374 kHz, $Ge_{28}Sb_{12}Se_{60}$ was found to have a nonlinear refractive index ~130 x fused silica and a two-photon absorption coefficient of 3.5 cm/GW. Given the large two-photon absorption coefficient, this material shows promise for optical limiting applications at 1 μm.

OCIS codes: (160.2750) Glass and other amorphous materials; (160.4330) Nonlinear optical materials; (190.4390) Nonlinear optics, integrated optics; (230.7380) Waveguides, channeled.

References and links

1. K. E. Stubkjaer, "Semiconductor optical amplifier-based all-optical gates for high-speed optical processing," IEEE J. Sel. Top. Quantum Electron. **6**(6), 1428–1435 (2000).
2. G. Steinmeyer, D. H. Sutter, L. Gallmann, N. Matuschek, and U. Keller, "Frontiers in ultrashort pulse generation: Pushing the limits in linear and nonlinear optics," Science **286**(5444), 1507–1512 (1999).
3. T. J. Kippenberg, R. Holzwarth, and S. A. Diddams, "Microresonator-based optical frequency combs," Science **332**(6029), 555–559 (2011).
4. J. S. Sanghera, C. M. Florea, L. B. Shaw, P. Pureza, V. Q. Nguyen, M. Bashkansky, Z. Dutton, and I. D. Aggarwal, "Non-linear properties of chalcogenide glasses and fibers," J. Non-Cryst. Solids **354**(2-9), 462–467 (2008).
5. B. J. Eggleton, B. Luther-Davies, and K. Richardson, "Chalcogenide photonics," Nat. Photonics **5**(3), 141–148 (2011).
6. A. Zakery and S. R. Elliot, "Optical properties and applications of chalcogenide glasses: a review," J. Non-Cryst. Solids **330**(1–3), 1–12 (2003).
7. P. Klocek and L. Columbo, "Index of refraction, dispersion, bandgap, and light scattering in GeSe and GeSbSe glasses," J. Non-Cryst. Solids **93**(1), 1–16 (1987).
8. P. Klocek, *Handbook of Infrared Optical Materials* (Marcel Dekker, Inc., 1991).
9. K. Ogusu, K. Suzuki, and H. Nishio, "Simple and accurate measurement of the absorption coefficient of an absorbing plate by use of the Brewster angle," Opt. Lett. **31**(7), 909–911 (2006).
10. J. Troles, F. Smektala, G. Boudebs, A. Monteil, B. Bureau, and J. Lucas, "Optical limiting behavior of infrared chalcogenide glasses," J. Optoelectron. Adv. Mater. **4**(3), 729–735 (2002).
11. M. Sheik-Bahae, A. A. Said, T. H. Wei, D. J. Hagan, and E. W. Van Stryland, "Sensitive measurement of optical nonlinearities using a single beam," IEEE J. Quantum Electron. **26**(4), 760–769 (1990).
12. M. Dinu, F. Quochi, and H. Garcia, "Third-order nonlinearities in silicon at telecom wavelengths," Appl. Phys. Lett. **82**(18), 2954–2956 (2003).
13. B. Gu, W. Ji, and X.-Q. Huang, "Analytical expression for femtosecond-pulsed z scans on instantaneous nonlinearity," Appl. Opt. **47**(9), 1187–1192 (2008).
14. R. W. Boyd, *Nonlinear Optics* (Academic Press, 2009).
15. M. Falconieri, "Thermo-optical effects in Z-scan measurements using high-repetition-rate lasers," J. Opt. A, Pure Appl. Opt. **1**(6), 662–667 (1999).
16. F. Ö. Ilday, J. R. Buckley, H. Lim, F. W. Wise, and W. G. Clark, "Generation of 50-fs, 5-nJ pulses at 1.03 μm from a wave-breaking-free fiber laser," Opt. Lett. **28**(15), 1365–1367 (2003).
17. M. Hass, J. W. Davisson, H. B. Rosenstock, and J. Babiskin, "Measurement of very low absorption coefficients by laser calorimetry," Appl. Opt. **14**(5), 1128–1130 (1975).
18. Vitron IG-5 Datasheet, http://www.vitron.de/datasheets/VITRON%20IG-5%20Datenblatt%20Jan%202015.pdf.

#228920 - $15.00 USD Received 3 Dec 2014; revised 4 Mar 2015; accepted 4 Mar 2015; published 18 Mar 2015

19. Schott Infrared Chalcogenide Glasses Datasheet, http://www.schott.com/advanced_optics/english/download/schott-infrared-chalcog-glasses-family-sheet-october-2013-eng.pdf.
20. K. Shinkawa and K. Ogusu, "Pulse-width dependence of optical nonlinearities in As_2Se_3 chalcogenide glass in the picosecond-to-nanosecond region," Opt. Express **16**(22), 18230–18240 (2008).
21. A. Ganjoo, H. Jain, C. Yu, J. Irudayaraj, and C. G. Pantano, "Detection and fingerprinting of pathogens: Mid-IR biosensor using amorphous chalcogenide films," J. Non-Cryst. Solids **354**(19-25), 2757–2762 (2008).
22. M. Olivier, J. C. Tchahame, P. Němec, M. Chauvet, V. Besse, C. Cassagne, G. Boudebs, G. Renversez, R. Boidin, E. Baudet, and V. Nazabal, "Structure, nonlinear properties, and photosensitivity of $(GeSe_2)_{100-x}(Sb_2Se_3)_x$ glasses," Opt. Mater. Express **4**(3), 525–540 (2014).
23. K. Tanaka and H. Hisakuni, "Photoinduced phenomena in As_2S_3 glass under sub-bandgap excitation," J. Non-Cryst. Solids **198–200**(1), 714–718 (1996).
24. T. Wang, X. Gai, W. Wei, R. Wang, Z. Yang, X. Shen, S. Madden, and B. Luther-Davies, "Systematic z-scan measurements of the third order nonlinearity of chalcogenide glasses," Opt. Mater. Express **4**(5), 1011–1022 (2014).
25. R. C. Miller, "Optical second harmonic generation in piezoelectric crystals," Appl. Phys. Lett. **5**(1), 17–19 (1964).
26. M. Sheik-Bahae, D. Crichton Hutchings, D. J. Hagan, and E. W. Van Stryland, "Dispersion of bound electronic nonlinear refraction in solids," IEEE J. Quantum Electron. **27**(6), 1296–1309 (1991).
27. Q. Zhang, W. Liu, L. Liu, L. Xu, Y. Xu, and G. Chen, "Large and opposite changes of the third-order optical nonlinearities of chalcogenide glasses by femtosecond and continuous-wave laser irradiation," Appl. Phys. Lett. **91**(18), 1–3 (2007).
28. W. Liu, Q. Zhang, L. Liu, L. Xu, Y. Xu, and G. Chen, "Enhancement of second-order optical nonlinearity in photo-darkened $Ge_{25}Sb_{10}S_{65}$ chalcogenide glass by femtosecond laser light," Opt. Commun. **282**(10), 2081–2084 (2009).
29. L. Petit, N. Carlie, H. Chen, S. Gaylord, J. Massera, G. Boudebs, J. Hu, A. Agarwal, L. Kimerling, and K. Richardson, "Compositional dependence of the nonlinear refractive index of new germanium-based chalcogenide glasses," J. Solid State Chem. **182**(10), 2756–2761 (2009).
30. K. Shimakawa, A. Kolobov, and S. R. Elliott, "Photoinduced effects and metastability in amorphous semiconductors and insulators," Adv. Phys. **44**(6), 475–588 (1995).
31. A. V. Kolovov, H. Oyanagi, K. Tanaka, and K. Tanaka, "Structural study of amorphous selenium by in situ EXAFS: Observation of photoinduced bond alternation," Phys. Rev. B **55**(2), 726–734 (1997).
32. A. V. Kolobov, H. Oyanagi, A. Roy, and K. Tanaka, "A nanometer scale mechanism for the reversible photostructural change in amorphous chalcogenides," J. Non-Cryst. Solids **232–234**(1), 80–85 (1998).
33. R. M. Almeida, L. F. Santos, A. Simens, A. Ganjoo, and H. Jain, "Structural heterogeneity in chalcogenide glass films prepared by thermal evaporation," J. Non-Cryst. Solids **353**(18–21), 2066–2068 (2007).
34. A. Ureña, A. Piarristeguy, M. Fontana, C. Vigreux-Bercovici, A. Pradel, and B. Arcondo, "Characterisation of thin films obtained by laser ablation of $Ge_{28}Se_{60}Sb_{12}$ glasses," J. Phys. Chem. Solids **68**(5–6), 993–997 (2007).
35. V. Balan, C. Vigreux, and A. Pradel, "Chalcogenide thin films deposited by radio-frequency sputtering," J. Optoelectron. Adv. Mater. **6**(3), 875–882 (2004).
36. J. Hu, V. Tarasov, N. Carlie, N.-N. Feng, L. Petit, A. Agarwal, K. Richardson, and L. Kimerling, "Si-CMOS-compatible lift-off fabrication of low-loss planar chalcogenide waveguides," Opt. Express **15**(19), 11798–11807 (2007).
37. M. Popovic, "Complex-frequency leaky mode computations using PML boundary layers for dielectric resonant structures," in Integrated Photonics Research, Vol. 91 of OSA Trends in Optics and Photonics (Optical Society of America, 2003), paper ITuD4.
38. F. P. Payne and J. P. R. Lacey, "A theoretical analysis of scattering loss from planar optical waveguides," Opt. Quantum Electron. **26**(10), 977–986 (1994).
39. R. G. DeCorby, N. Ponnampalam, M. M. Pai, H. T. Nguyen, P. K. Dwivedi, T. J. Clement, C. J. Haugen, J. N. McMullinm, and S. O. Kasap, "High index contrast waveguides in chalcogenide glass and polymer," IEEE J. Sel. Top. Quantum Electron. **11**(2), 539–546 (2005).
40. T.-K. Liang and H.-K. Tsang, "Nonlinear absorption and raman scattering in silicon-on-insulator optical waveguides," IEEE J. Sel. Top. Quantum Electron. **10**(5), 1149–1153 (2004).
41. F. Smektala, C. Quemard, V. Couderc, and A. Barthélémy, "Non-linear optical properties of chalcogenide glasses measured by Z-scan," J. Non-Cryst. Solids **274**(1–3), 232–237 (2000).
42. B. Gu, Y.-X. Fan, J. Chen, H.-T. Wang, J. He, and W. Ji, "Z-scan theory of two-photon absorption saturation and experimental evidence," J. Appl. Phys. **102**(8), 083101 (2007).
43. J.-F. Lami, P. Gilliot, and C. Hirlimann, "Observation of interband two-photon absorption saturation in CdS," Phys. Rev. Lett. **77**(8), 1632–1635 (1996).
44. G. Lenz, J. Zimmermann, T. Katsufuji, M. E. Lines, H. Y. Hwang, S. Spälter, R. E. Slusher, S.-W. Cheong, J. S. Sanghera, and I. D. Aggarwal, "Large Kerr effect in bulk Se-based chalcogenide glasses," Opt. Lett. **25**(4), 254–256 (2000).

1. Introduction

Nonlinear optical effects can be useful for a number of applications, including ultrafast all-optical switching [1], short pulse generation [2], and frequency combs [3]. Chalcogenide

#228920 - $15.00 USD Received 3 Dec 2014; revised 4 Mar 2015; accepted 4 Mar 2015; published 18 Mar 2015

glasses, which contain a chalcogen element such as S, Se, or Te covalently bonded to at least one other element, are a promising platform for compact, low threshold nonlinear optical devices operating at near- to mid-infrared wavelengths. They have high nonlinearities [4], transparencies up to 20 μm [5], and large figures of merit (ratio of nonlinearity to two-photon absorption) [6]. We focus specifically on the chalcogenide glass $Ge_{28}Sb_{12}Se_{60}$ because of its As-free composition, large band gap [7], transparency to 14 μm [8], and high glass transition temperature of 300°C [8]. To date, most work characterizing this material's nonlinear optical properties has centered on telecom wavelengths. A better understanding of this material over a wider wavelength range in both bulk and waveguide forms is crucial for leveraging its nonlinear properties in device designs.

In this letter, we characterize the linear and nonlinear optical properties of $Ge_{28}Sb_{12}Se_{60}$ bulk samples and waveguides at a wavelength of 1.03 μm. We find that the fabricated waveguides have properties that are similar to that of bulk and are well-suited for optical limiting in this spectral region.

2. Optical characterization of bulk $Ge_{28}Sb_{12}Se_{60}$

The linear absorption of bulk $Ge_{28}Sb_{12}Se_{60}$ (commercially available) was determined to be $\alpha = 0.27 \pm 0.03$ cm^{-1}, or 1.17 dB/cm, at a wavelength of 1.03 μm from measurements of the reflected and transmitted power at Brewster's angle, using a technique described by Ogusu et al. [9]. Similar measurements on a reference sample As_2Se_3 agreed with values in literature [10].

The nonlinear refractive index n_2 and two-photon absorption coefficient β of polished Ge-Sb-Se bulk samples were measured using the z-scan technique [11], in which a sample is translated through the focus of a Gaussian beam, and the transmission through a circular aperture, placed in the far field, is recorded. Measurement of the transmission as a function of position without the aperture allows for determination of β. For a Gaussian pulse shape, transmission without the aperture is given by

$$T_{open} = \sum_{m=0}^{\infty} \frac{[-q_0(z)]^m}{(m+1)^{3/2}}, \tag{1}$$

for values of $|q_0| < 1$, where $q_0 = \beta I_0 L_{eff}/(1 + x^2)$, $x = z\lambda/(\pi w^2)$, z is the distance of the sample from focus, and m is an integer [11]. Here, I_0 is the peak on-axis intensity, w is the beam waist, λ is the wavelength, and the effective sample length, $L_{eff} = (1\text{-}e^{-\alpha L})/\alpha$, where L is the physical sample length and α is the linear absorption coefficient. Typically $q_0 << 1$, and only the first two terms of Eq. (1) contribute significantly. For larger values of q_0, additional terms were included to ensure accuracy within 0.5%. For small refractive and absorption changes, transmission through a partially closed aperture is given by

$$T_{cl} \cong 1 + \frac{4x\langle \Delta\varphi_0 \rangle}{(1+x^2)(9+x^2)} - \frac{\beta I_0 L_{eff}(3-x^2)}{2\sqrt{2}(1+x^2)(9+x^2)}, \tag{2}$$

where the time-averaged peak on-axis phase shift is given by $\langle \Delta\varphi_0 \rangle = 2\pi L_{eff} n_2 I_0 (1\text{-}S)^{0.25}/(2)^{0.5}$ for a Gaussian pulse shape, and S is the aperture transmission [12]. Larger changes can be fit with a full expression given by Gu et al. [13].

A number of physical processes, including electronic polarization, thermal effects, and free-carrier effects, can cause a nonlinear change in the refractive index, but their corresponding response times and magnitudes vary greatly [14]. Nonlinear changes due to electronic polarization are of particular interest, given their fast, fs response times. Although the z-scan technique only measures the magnitude and sign of the nonlinearity, measurements at different repetition rates can help distinguish the origin of the nonlinearity [15].

The light source used in these experiments was a mode-locked Yb-doped fiber laser operating at a 37.4 MHz repetition rate, with ~200 fs Gaussian pulses at a central wavelength of 1.03 μm, modeled after a design by Ilday et al. [16]. An acousto-optic modulator (AOM)

#228920 - $15.00 USD Received 3 Dec 2014; revised 4 Mar 2015; accepted 4 Mar 2015; published 18 Mar 2015

was used as a pulse-picker to reduce the repetition rate to 374 kHz. A circuit containing a high speed comparator, counter, and logic gates was designed to provide a fast, low duty cycle trigger signal necessary to drive the AOM. Data was taken at these two repetition rates (37.4 MHz and 374 kHz) with circularly polarized light, on 2 mm-thick polished bulk $Ge_{28}Sb_{12}Se_{60}$ samples. A series of open and closed aperture z-scan traces were taken over a range of intensities from 20 to 95 MW/cm^2. To account for sample inhomogeneities, z-scan traces were divided by background traces taken at very low intensity levels, where the nonlinearity would produce negligible effects. No changes or degradation to the sample surface were observed in between or after measurements at the different repetition rates.

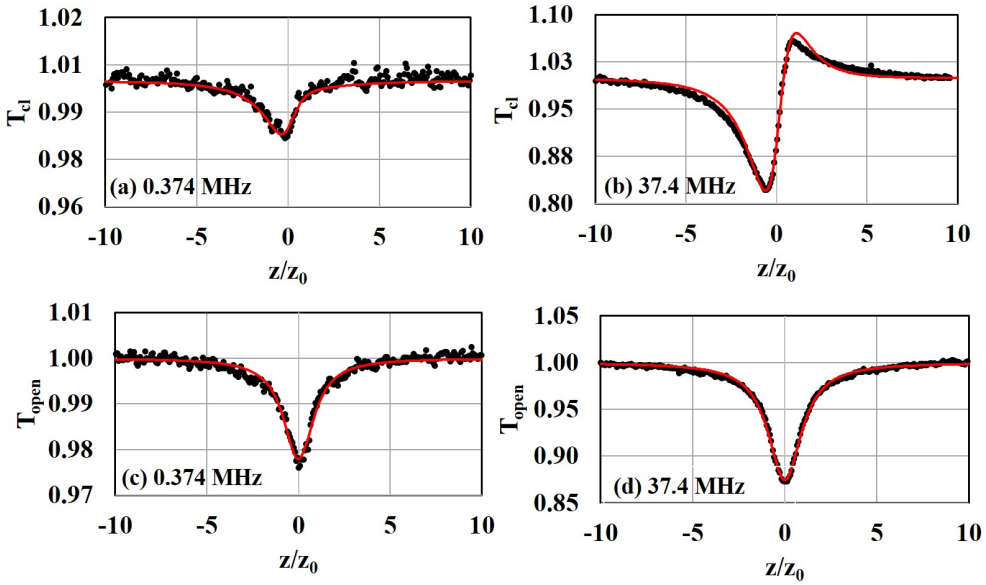

Fig. 1. Example closed aperture (a) and (b) and open aperture (c) and (d) z-scan traces taken on $Ge_{28}Sb_{12}Se_{60}$. Note that the traces on the left, (a) and (c), were taken at 0.374 MHz with I_0 = 88.5 MW/cm^2. The traces on the right, (b) and (d) were taken at 37.4 MHz with I_0 = 35 MW/cm^2. Data is shown by the black points, and the fits are represented with red lines.

Example z-scan traces at the two different repetition rates are shown in Fig. 1. At the lower repetition rate, a noticeably smaller change in transmission was observed for both the open and closed aperture z-scans, and large two-photon absorption obscured the typical valley-peak shape of the closed aperture z-scan.

The fit values for the data at the two repetition rates, taken over a range of intensities, are summarized in Fig. 2. Errors in β and n_2 are approximately 11% and 20%, respectively. The main sources of error in the measurements were laser power fluctuations and uncertainty in the pulse width. At the high repetition rate, n_2 is enhanced, ranging from 15 to 21x10^{-17} m^2/W, and increases slightly with increasing intensity, while the value of β, roughly 30 cm/GW, also appears significantly enhanced. At the lower repetition rate, both n_2 and β show no dependence on intensity, as expected.

We investigated whether the repetition rate dependence could be caused by thermal effects, where the refractive index changes due to the thermo-optic coefficient and sample heating from absorption. The temperature change, ΔT of the sample due to linear absorption α is given by $\Delta T = \alpha L_s P_0 t/(MC_p)$, where L_s is the sample length, P_0 is the incident power, M is the sample's mass, C_p is the specific heat, and t is the bulk heating transit time [17]. For a disk-shaped sample, t is given by $t = r^2/(6\kappa)$, where r is the radius and κ is the thermal diffusivity [17]. Using the material values for our $Ge_{28}Sb_{12}Se_{60}$ sample (α = 0.27 cm^{-1}, L_s = 2 mm, r = 1.27 cm, M = 4.72g, κ = 0.1626 mm^2/s, t = 165.4 s, C_p = 0.33 J/g-K) [18], we

#228920 - $15.00 USD Received 3 Dec 2014; revised 4 Mar 2015; accepted 4 Mar 2015; published 18 Mar 2015

calculate ΔT~0.011-0.057 K for the P_0~2-10 mW used at the high repetition rate of 37.4 MHz, and we calculate ΔT~4.6-6.9 x 10^{-4} K for the P_0~80-120 μW used at the lower repetition rate of 0.374 MHz. Using the thermo-optic coefficient dn/dT = 78.8x10^{-6}/K for $Ge_{28}Sb_{12}Se_{60}$ at λ = 1μm [19], we estimate corresponding change in refractive index from these absorption-induced temperature changes to be 0.9-4.5 x 10^{-6} at the high repetition rate, and 4.6-6.9 x 10^{-8} at the low repetition rate. In comparison, the measured index changes, $dn = n_2 I_0$, from the z-scan for the high and low repetition rates were 0.3-1.67 x 10^{-4} and 2.6-3.2 x 10^{-6} respectively, nearly two orders of magnitude larger than what we'd expect from thermal effects. From these calculations, effects due to the thermo-optic coefficient are insignificant, contributing only a few percent of the total measured change in refractive index at both repetition rates. While others have observed cumulative nonlinearities from free-carrier refractive and dispersive contributions in chalcogenide glasses, these are expected to be negligible at both repetition rates due to the short pulse durations used [20].

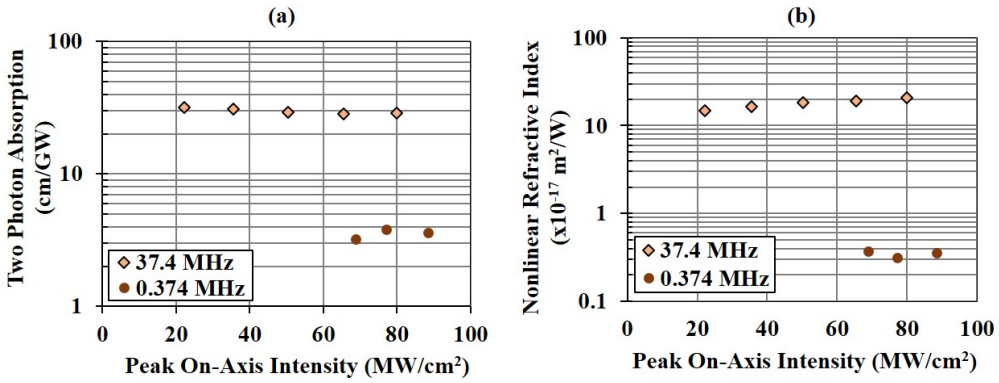

Fig. 2. Plots of (a) two-photon absorption coefficient, β and (b) nonlinear refractive index, n_2 of $Ge_{28}Sb_{12}Se_{60}$ as a function of peak on-axis intensity, measured by the z-scan technique for two repetition rates, 0.374 MHz and 37.4 MHz. Errors in β and n_2 are approximately 11% and 20%, respectively. At 0.374 MHz, β = 3.5 cm/GW and n_2 = 3.4x10^{-18} m^2/W. Enhanced values of β and n_2 observed at the higher repetition rate are believed to be a cumulative effect caused by the photosensitivity of the material.

One possible origin of additional nonlinearities includes effects from photosensitivity, which we will now discuss in more depth. A variety of Ge-Sb-Se glasses and other chalcogenides have been shown to exhibit photodarkening, in which the band gap red-shifts and absorption and refractive index increase upon illumination close to the band edge [21–23]. Miller's Rule, which relates the linear refractive index n_0 to n_2, predicts that the increase in n_0 from photodarkening would increase n_2 [24,25]. Additionally, Sheik Bahae's model for the dispersion of n_2 and β predicts that a decrease in band gap energy, such as that produced by photodarkening, will increase both n_2 and β [26]. Indeed, an increase in n_2 after photodarkening with a fs laser has been observed in other chalcogenides, such as Ge-Sb-S and As_2S_3 [27,28]. Since the magnitude of the property changes from photodarkening can depend on illumination characteristics, these changes could also produce an effective cumulative nonlinearity [20]. In the case of Ge-Sb-Se glass, one would expect that a red-shift in the band edge would lead to higher two-photon absorption and higher linear and nonlinear refractive indices, consistent with the direction of the shift we observe at the higher repetition rate. Given this, along with the magnitudes measured, the enhanced effective β and n_2 at the higher repetition rate were likely caused by a cumulative effect stemming from photosensitivity.

From the data at the lower repetition rate, we measure n_2 = 3.4 ± 0.4x10^{-18} m^2/W and β = 3.5 ± 0.2 cm/GW on the $Ge_{28}Sb_{12}Se_{60}$ sample for circularly polarized light. These results at the lower repetition rate are independent of intensity, and of the same order of magnitude as those seen for other chalcogenides, even for experiments using short pulses at much lower

#228920 - $15.00 USD Received 3 Dec 2014; revised 4 Mar 2015; accepted 4 Mar 2015; published 18 Mar 2015

repetition rates on the order of 1 kHz to 10 Hz [22,24,29]. For example, Petit et al. measured n_2 = 11.5 ± 3x10^{-18} m^2/W and β = 4.9 ± 0.6 cm/GW for $Ge_{28}Sb_7Se_{65}$ using the z-scan technique with a 15 ps, 10 Hz Nd:YAG at 1.064 μm [29]. Since photorefractive effects often lead to very strong nonlinear responses and can be intensity-dependent, this comparison and lack of intensity-dependence strongly suggests the 0.375 MHz results include only the two photon absorption and Kerr effect. A time-resolved method such as pump-probe will not be able to determine the origin of the nonlinearity, because photodarkening can produce both cumulative nonlinearities, as well as ultrafast nonlinearities due to changes in the band gap energy, as discussed earlier. Photosensitivity-induced changes can be clearly identified by changes in bond structure [30–32]. Thus, a technique capable of sensing structural changes, such as a Raman spectroscopy or X-ray absorption spectroscopy, may more directly probe the presence of photosensitivity [30–32], but it is beyond the scope of this paper.

For $Ge_{28}Sb_{12}Se_{60}$, we calculate a figure of merit, $FOM = n_2/(\beta\lambda)$ of 0.094 at 1.03 μm. While the low *FOM* indicates that the glass is not well-suited for switching applications at 1 μm, the high β suggests promise for optical limiting applications in this spectral region.

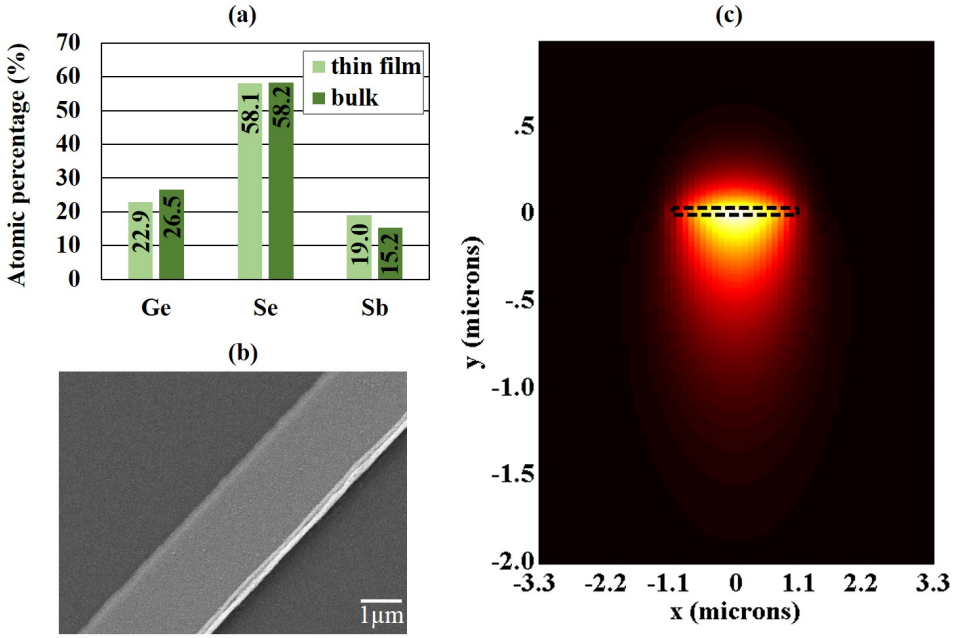

Fig. 3. (a) Atomic composition of thin film and bulk Ge-Sb-Se samples. (b) Scanning electron micrograph of a chalcogenide strip waveguide, consisting of silicon substrate, 3-μm-thick SiO_2, a 2.2-μm-wide and 45-nm-thick Ge-Sb-Se layer, and air upper cladding. (c) Simulated mode profile for the single-mode Ge-Sb-Se strip waveguide. The black dotted rectangular outline indicates the x and y position and size of the Ge-Sb-Se core relative to the mode.

3. Waveguide fabrication

For thin film devices, chalcogenides are typically prepared in bulk glass form and then deposited onto a substrate using thermal evaporation [33], pulsed laser deposition [34], or sputtering [35]. Thermal evaporation is a particularly attractive, simple technique that yields high quality films. To fabricate waveguides, we thermally evaporated $Ge_{28}Sb_{12}Se_{60}$ glass onto a Si wafer with a 3 μm oxide layer and used lift-off to pattern strip Ge-Sb-Se waveguides of 2.2 μm width and 45 nm height.

Energy Dispersive X-ray Spectroscopy (EDS) measurements on thin Ge-Sb-Se films confirmed that the stoichiometry of the fabricated thin films is within 4 atomic % of the bulk material, as shown in Fig. 3(a). The waveguide dimensions were chosen to ensure single-

#228920 - $15.00 USD Received 3 Dec 2014; revised 4 Mar 2015; accepted 4 Mar 2015; published 18 Mar 2015

mode operation at 1.03 μm and enable quick, straightforward patterning with photolithography, rather than electron-beam lithography. Figure 3(b) shows a scanning electron micrograph (SEM) of the fabricated waveguides. The surface roughness was measured to be 0.8 nm using atomic force microscopy (AFM). The average sidewall roughness was measured to be 11.8 nm using data from high resolution SEMs. These measured roughness values are comparable to values obtained by other groups using a similar fabrication process [36].

4. Waveguide characterization

Light was coupled in and out of the Ge-Sb-Se waveguides using high numerical aperture (NA = 0.35) fibers mounted on piezo-actuated three-axis stages for precise alignment. Horizontally polarized light was used to match the polarization of the guided mode. The linear loss of the Ge-Sb-Se waveguides was measured by coupling low power, cw light into a given waveguide, and recording the intensity of the light scattered above the waveguide surface as a function of distance along the waveguide using a CCD image sensor. The intensity of the scattered light is proportional to the intensity of the light remaining in the waveguide, and thus a fit of the scattered light intensity vs. distance curve to a decaying exponential will yield the total loss. A linear loss measurement on one waveguide is shown in Fig. 4. Averaging over measurements on six adjacent waveguides, the linear loss was determined to be 11.9 ± 1 dB/cm. Note that the loss measurement includes material absorption, as well as scattering loss from the surface and sides of the waveguide.

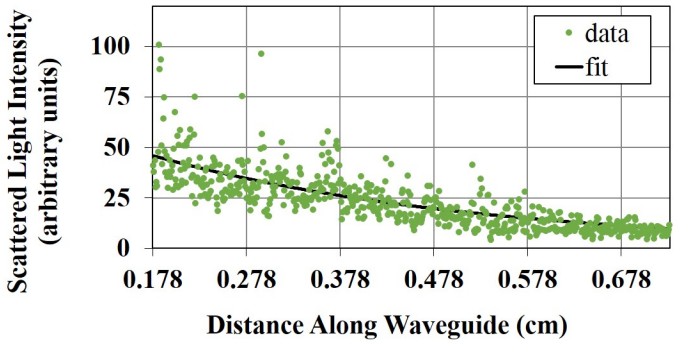

Fig. 4. Plot of scattered light intensity vs. distance for a single-mode Ge-Sb-Se waveguide at a wavelength of 1.03 μm. A fit to a decaying exponential yields a total loss of 2.8 ± 0.3 cm^{-1}, or 12.2 dB/cm, for the waveguide illustrated. An average total loss of 11.9 ± 1 dB/cm is obtained for measurements on six adjacent waveguides.

The waveguide loss due only to material absorption is given by $\alpha_{wg,mat} = \iint \alpha(x,y)\,|E(x,y)|^2\,dxdy \,/\, \iint |E(x,y)|^2 dxdy$, where $E(x,y)$ is the x-component of the electric field of the TE mode at the location (x,y) in the waveguide cross section and $\alpha(x,y)$ is the material linear absorption at the location (x,y). Since the fabricated thin films appear to have similar composition to the bulk, we expect that the material absorption of the waveguide core material is similar to that of the bulk glass, 0.27cm^{-1} or 1.17 dB/cm. The under cladding SiO_2 material has negligible absorption at 1.03 μm. Simulating the electric field of the guided TE mode [37] and calculating the overlap integral of the field with the linear absorption, we estimate loss in the waveguide from material absorption to be 0.15 dB/cm, leaving ~11.75 dB/cm of loss due to scattering. Note that the contribution of material loss to the total waveguide loss is low due to the weak ~13% confinement of the mode to the core material.

Due to the asymmetric waveguide geometry, the electric field of the guided mode is very weak near the sidewalls of the waveguide, but it is strong near the surface, as illustrated in Fig. 3(c). Thus, we expect scattering loss due to surface roughness, rather than sidewall

#228920 - $15.00 USD Received 3 Dec 2014; revised 4 Mar 2015; accepted 4 Mar 2015; published 18 Mar 2015

roughness, to dominate. Approximating the waveguide as a slab waveguide and following the theory of Payne and Lacey [38], the scattering loss due to 0.8 nm surface roughness is expected to be on the order of 13 dB/cm. This calculation is consistent with our measurements. For comparison, etched high-contrast, chalcogenide-based embedded strip waveguides have been shown to have losses ~10-15 dB/cm [39]. Measurements made at 1550 nm on single-mode thermally-evaporated chalcogenide waveguides with significantly smaller core aspect ratios suggest that lower losses on the order of 2-6 dB/cm for strip waveguides and < 0.5 dB/cm for rib waveguides are possible [36]. While our measured loss is reasonable for the given design, we expect the scattering loss of Ge-Sb-Se waveguides can be similarly reduced by optimizing the design of the strip waveguide cross section dimensions to decrease the field at the surface and thereby decrease scattering loss, or by using a rib waveguide design.

Loss in a waveguide due to both linear absorption and two-photon absorption is described by the following equation:

$$\frac{1}{T} = \frac{[1-e^{-\alpha L_{wg}}]\beta_{wg}}{\alpha} I + e^{\alpha L_{wg}}, \tag{3}$$

where $1/T$ is the reciprocal transmission, I is the incident peak intensity, α is the linear absorption of the waveguide, β_{wg} is the two-photon absorption coefficient of the waveguide, and L_{wg} is the length of the waveguide [40]. At high intensities, saturation of the two-photon absorption has been observed in chalcogenide materials [41,42], and it can be modeled with a saturation intensity I_{sat} and an effective two-photon absorption coefficient, $\beta_{eff} = [1 + I/I_{sat}]^{-1}\beta_{wg}$ [43]. The nonlinear loss of Ge-Sb-Se waveguides was measured by coupling linearly polarized, 7 ps-long pulses from a Yb-doped fiber laser at a 37.4 MHz repetition rate into 6 mm-long waveguides and measuring the output intensity as a function of input intensity. To determine the coupling loss at the input and output waveguide facets, measurements were made launching light forwards through the waveguide, and then backwards, switching input and output fiber patch cord connectors while leaving the high numerical aperture coupling fibers fixed in position. Figure 5 shows the reciprocal transmission as a function of incident peak intensity. Since saturation became noticeable at intensities around 1 GW/cm^2, data was fit to Eq. (3), replacing β_{wg} by β_{eff} and using β_{wg}, α, and I_{sat} as fitting parameters. Earlier independent measurements of α for the waveguides agreed with values from fits. An average of fits to three data sets yields β_{wg} = 11.5 ± 0.7 cm/GW and I_{sat} = 4.3 ± 0.7 GW/cm^2 for the waveguides. The main sources of uncertainty are the measured output power and coupling efficiency.

When comparing nonlinearities measured in the waveguides to those measured in bulk, the polarization, waveguide confinement factor, and illumination conditions must all be taken into account. For amorphous materials, both n_2 and β depend on polarization, with $n_2^{circ} = 2n_2^{lin}/3$ and $\beta^{circ} = 2\beta^{lin}/3$, where n_2^{circ} and β^{circ} are values for circular polarization, and n_2^{lin} and β^{lin} are values for linear polarization [14]. To estimate the expected nonlinearity of the waveguide structure, the overlap of the guided mode with the core and cladding layers was calculated, weighting each with the appropriate nonlinear material properties for linear polarization, under similar 37.4 MHz repetition rate illumination conditions. In particular, $\beta_{wg} = \iint \beta(x,y) \,|\, E(x,y) \,|^2 \, dxdy \,/\, \iint |E(x,y)|^2 \, dxdy$, where $E(x,y)$ is the x-component of the electric field of the TE mode at the location (x,y) in the waveguide cross section, and $\beta(x,y)$ is the material two-photon absorption coefficient at the location (x,y). From this calculation, we would expect β_{wg} to be 5.8 cm/GW. This value is within a factor of 2 of our measured value for the waveguides. It is important to note that small changes in composition of Ge-Sb-Se glasses have been shown to greatly affect the two-photon absorption coefficient near 1 μm, with β increasing with increasing Sb content [22]. Given the small but measurable differences in stoichiometry, shown in Fig. 3(a), we expect the difference in β can be explained by the

#228920 - $15.00 USD Received 3 Dec 2014; revised 4 Mar 2015; accepted 4 Mar 2015; published 18 Mar 2015

slight increase in Sb-content and decrease in Ge-content in our fabricated waveguides compared to the bulk.

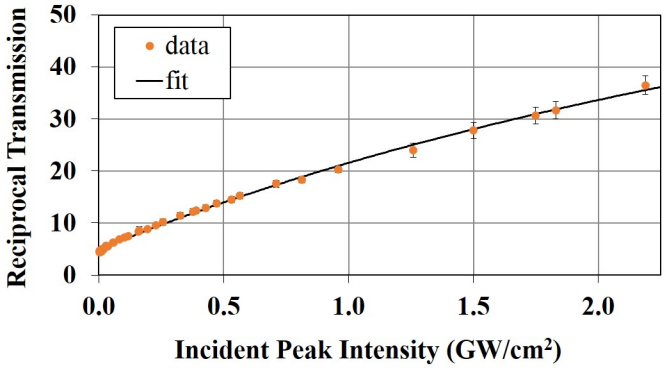

Fig. 5. Plot of reciprocal transmission as a function of incident peak intensity for a single-mode Ge-Sb-Se waveguide. The average effective two-photon absorption coefficient of the waveguide is measured to be 11.5 ± 0.7 cm/GW.

The input and output spectra from our waveguides were also measured, revealing a weak, power-dependent broadening of the spectral full-width at half-maximum (FWHM). Estimates of spectral broadening from split-step numerical solutions to the Nonlinear Schrödinger Equation, using the expected effective n_2 for the waveguide and measured β_{wg} with saturation, suggest the changes in FWHM are predominately due to β selectively decreasing the high-intensity peak of the pulses, making accurate determination of n_2 for the waveguide difficult.

5. Conclusion

In summary, we fabricated single-mode, air-clad, strip Ge-Sb-Se waveguides with similar composition and properties to bulk $Ge_{28}Sb_{12}Se_{60}$ glass. In bulk, using a reduced 374 KHz repetition rate, $n_2 = 3.4 \pm 0.4 \times 10^{-18}$ m^2/W and $\beta = 3.5 \pm 0.2$ cm/GW. In the waveguides, the linear loss, 11.9 dB/cm on average, was dominated by scattering loss. The nonlinear loss of the fabricated waveguides was 11.5 cm/GW, reasonable considering the enhanced value of β with the 37.4 MHz repetition rate, the overlap of the mode with the waveguide structure, and slight variations in composition. We expect changes in waveguide geometry to increase the power confined in the chalcogenide core can help to both reduce the effect of scattering loss and increase the effective nonlinearity of the waveguide.

Although two-photon absorption for the bulk and the waveguides is large at 1 μm and will limit the realm of nonlinear device applications in this wavelength regime, Lenz et al. have shown that the figure of merit improves substantially at 1550 nm, farther from the band edge of the material [44]. In the future, we plan to optimize, fabricate, and characterize Ge-Sb-Se waveguide devices at 1550 nm and 3000 nm, where we anticipate the material will not suffer from large nonlinear absorption.

Acknowledgments

The authors acknowledge the financial support from NSF grant EECS-1232077 and the University of Colorado Boulder Innovative Seed Grant Program. The authors are grateful for technical discussions with Peter Rakich (Yale) and Tymon Barwicz (IBM). Additionally, the authors thank Milos Popovic (University of Colorado Boulder) for technical discussions and use of his waveguide mode solver [37]. M. Krogstad was supported by the Department of Defense (DoD) through the National Defense Science & Engineering Graduate Fellowship (NDSEG) Program. Publication of this article was funded by the University of Colorado Boulder Libraries Open Access Fund.